Energy 335 (2025) 137962

Contents lists available at ScienceDirect

Energy

journal homepage: www.elsevier.com/locate/energy

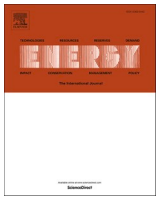

Micro-overcharge driven nonlinear degradation mechanisms: Towards early detection of capacity knee points in lithium-ion batteries

Xiaoli Ma [a,b,1], Sheng Fang [a,1], Xueling Shen [a], Hang Zhang [a], Fengling Yun [a], Min Gao [a], Zhanglong Yu [a,*], Yanyan Fang [a,**], Fang Lian [b,***]

[a] China Automotive Battery Research Institute Co., Ltd., Beijing, 101407, PR China
[b] School of Materials Science and Engineering, University of Science and Technology Beijing, Beijing, 100083, PR China

ARTICLE INFO

Handling editor: X Ou

Keywords:
Lithium-ion batteries
Micro-overcharging
Nonlinear degradation
MO-DIC method
Lifespan prediction

ABSTRACT

Predicting capacity decay in lithium-ion batteries is challenging, especially with nonlinear degradation patterns. This study introduces a novel approach by investigating the capacity decay characteristics of lithium-ion batteries under prolonged micro-overcharging, revealing distinct peaks in the incremental capacity (IC) curve indicative of accelerated cathode material degradation. Furthermore, we propose the Micro-Overcharge Differential Incremental Capacity (MO-DIC) method, a pioneering technique for predicting the capacity decay knee point. MO-DIC uses the rate of change of normalized peak height in the differential overcharging IC curve as a predictive indicator. Validated with low N/P ratio batteries, MO-DIC forecasts the life inflection point 25 to 36 cycles ahead of capacity fade indicators and approximately 50 cycles before end-of-life. This innovative approach markedly improves battery health status prediction, offering substantial benefits for battery life cycle analysis and proactive maintenance strategy formulation. Future work will refine the MO-DIC method and evaluate its applicability across diverse battery types and operating conditions.

1. Introduction

Lithium-ion batteries have garnered widespread acclaim for their high energy density, superior power output, and extended service life, thereby becoming the preeminent energy storage solution in electric vehicles (EVs) and energy storage systems [1–3]. These attributes have propelled lithium-ion batteries to the forefront of energy storage technologies, making them indispensable in modern applications where high performance and reliability are paramount. However, despite their many advantages, lithium-ion batteries are not immune to degradation. Over extended cycling, some abnormal lithium-ion batteries may experience a progressive decline in capacity, often manifesting as non-linear decay patterns [4]. This phenomenon, commonly referred to as capacity fade, is characterized by a precipitous drop in capacity over time [5–7]. The non-linear nature of this aging process poses significant challenges to the safety, longevity, and residual value of the batteries, as well as their suitability for cascaded utilization [8,9]. Moreover, non-linear aging can compromise the functionality of online battery management systems (BMSs), diminishing the precision of the state of charge (SOC) and state of health assessments [10,11]. Therefore, it is imperative to assess the non-linear decay characteristics of abnormal lithium-ion batteries to enhance predictive capabilities and management strategies.

The prediction of lithium-ion battery capacity has been significantly advanced by the advent of model-based and data-driven methodologies. Model-based approaches, which encompass empirical and physical models, simulate the aging behaviors of batteries based on intrinsic degradation mechanisms [12,13]. Li et al. employed an improved bat algorithm optimization kernel extreme learning machine to predict lithium-ion battery life, thereby enhancing the safety and stability of battery usage [14]. These methodologies rely on a thorough understanding of the degradation processes and/or the utilization of purely mathematical strategies to define the degradation profiles of batteries, encompassing voltage and health life metrics. However, the health life of

* Corresponding author.
** Corresponding author.
*** Corresponding author.
E-mail addresses: yuzl@glabat.com (Z. Yu), fangyy@glabat.com (Y. Fang), lianfang@mater.ustb.edu.cn (F. Lian).
[1] These authors contributed equally.

https://doi.org/10.1016/j.energy.2025.137962
Received 4 July 2025; Received in revised form 22 July 2025; Accepted 7 August 2025
Available online 7 August 2025

a battery is invariably influenced by a variety of factors, especially for abnormal batteries with non-linear degradation. Given the intricate, non-linear characteristics inherent in degradation, data-driven methods, despite their proficiency in capturing statistical regularities, often fail to adequately characterize the non-linear and dynamic aspects of battery aging [15]. The integration of implicit degradation features, such as incremental capacity, can significantly improve the accuracy and efficiency of data-driven methods [16]. Incremental capacity analysis (ICA), utilizing the capacity-voltage curve, offers a quantitative analysis of lithium inventory loss (LLI) and active material loss (LAM). This approach extracts electrochemical signal features associated with these failure modes [17–19]. Studies have suggested that the characteristics of the incremental capacity (IC) curve, including the peak shape, height, and position, may be closely linked to the capacity decay and aging mechanisms of lithium-ion batteries [20–22]. For example, a reduction in the IC peak height post-cycling aging was found to be correlated with the loss of active material, and a decrease in lithium inventory could rapidly lower peak height [23]. Consequently, the peak height and position derived from the IC curve may act as indirect characteristic parameters to delineate the health status of the battery, and are critical in the prediction of knee point. However, the ICA method, which employs low current rates such as C/25 and C/6, remains challenged by the need to minimize the impact of ohmic resistance on peak voltage changes to capture subtle signals during the process [22]. This requirement significantly compromises the timeliness and precision of this method, highlighting an urgent need for rapid and cost-effective techniques that can handle the fast charging demand of batteries. Therefore, there is a pressing need to develop advanced methodologies that can accurately predict the non-linear degradation of lithium-ion batteries, particularly in the context of their complex aging behaviors and the practical constraints of real-world applications.

Despite the advancements in predictive methodologies discussed earlier, understanding the root causes of nonlinear capacity degradation in lithium-ion batteries is essential for developing robust predictive and management strategies. One significant factor contributing to this degradation is micro-overcharging, which has garnered increasing attention due to its subtle yet impactful effects on battery health [24, 25]. Unlike overcharging [26], which results from complete BMS failure or human error and leads to severe and immediately noticeable consequences such as rapid voltage rise, electrolyte decomposition, gas generation, and potential thermal runaway or explosion, micro-overcharging involves a slight increase in the charging cut-off voltage. This subtle overcharge causes gradual capacity loss over time, primarily through lithium plating on the anode and an increase in internal resistance. The effects of micro-overcharging accumulate subtly over multiple charge-discharge cycles, making it difficult to detect and manage. It can stem from slight BMS miscalibration, high-temperature charging conditions, or manufacturing inconsistencies, such as minor deviations in the N/P ratio (the mole ratio of active materials in the negative to positive electrodes) [27]. The insidious nature of micro-overcharging makes it particularly challenging to address. While overcharging poses immediate safety risks and can be mitigated through robust safety measures and user education, micro-overcharging's cumulative effects require more sophisticated detection and management strategies. Precise voltage and current monitoring, advanced diagnostic algorithms, and adaptive control strategies are essential for mitigating the long-term damage caused by micro-overcharging [28]. Given its potential to erode battery performance and safety over time, micro-overcharging underscores the critical need for early warning monitoring technologies to enhance battery safety and longevity.

In this study, we introduce a groundbreaking approach to understanding and predicting nonlinear capacity degradation in lithium-ion batteries through the lens of micro-overcharging. Unlike conventional methods relying on standard IC curves, our research pioneers the Micro-Overcharge Differential Incremental Capacity (MO-DIC) analysis. This innovative technique integrates controlled micro-overcharging scenarios with advanced DIC methodology to uncover unique degradation signatures. Our comprehensive experiments and data-driven analysis elucidate the specific mechanisms of micro-overcharging-induced degradation and establish a robust predictive model. This model significantly enhances the reliability and safety of lithium-ion battery systems, offering a transformative tool for proactive battery health management and optimized lifecycle utilization. Specifically, this study aims to develop an early prediction technique for the nonlinear capacity degradation inflection point of lithium-ion batteries based on the MO-DIC method.

2. Methodology

The methodology we used to process the data and extract the degradation features are overviewed in Fig. 1. We based this workflow on our experimental results in order to optimize the extraction of degradation features, as will be further detailed in the later sections of this report.

2.1. Capacity fade features

To identify a battery degradation behavior, its SOH must first be calculated. The capacity retention rate is used to describe the SOH, according to the relationship:

$$SOH = \frac{Capacity_{fade}}{Capacity_{original}} \quad \text{Eq. 1}$$

The capacity retention curve typically exhibits a knee point, where the battery capacity changes from slowly declining to rapidly decreasing. The shape of this curve varies significantly based on each battery type and its particular electrochemical properties. As a result, mathematical methods are developed with a focus on locating the knee point. Based on research [23], the curvature at any point in a continuous function can be defined using its first and second derivatives, using the relationship:

$$K_f(x) = \frac{f''(x)}{(1 + f'(x)^2)^{1.5}} \quad \text{Eq. 2}$$

This formula matches the point of maximum curvature to ad hoc operators use to select a knee point, since curvature is a mathematical measure of how much a function differs from a straight line. Maximum curvature therefore captures the levelling-off effect that operators use to identify the knee point, which is then given by the point where the derivative is at its maximum value.

2.2. Differential capacity and voltage features

The capacity retention rate can be used to visualize battery degradation, but it cannot reflect the mechanism underlying this degradation—and therefore cannot be used to make predictions. Therefore, another approach must be used to fully describe the features of a battery degradation. The differential capacity and voltage (IC) curves are commonly used to identify different battery degradation mechanisms, such as loss of active materials, based on numerical analysis. The IC curve is defined by the following equation.

$$\frac{dQ}{dV} = \frac{Capacity_i - Capacity_{i-1}}{Voltage_i - Voltage_{i-1}} \quad \text{Eq. 3}$$

which relies on the difference in value between two sampling points. For raw data that is sampled every second, this can introduce challenges as the noise for each measurement will be further amplified when calculated the difference. Denser sampling also leads to a higher frame number, resulting in noisier curves. Such a curve cannot be used to identify the features. Thus, first is necessary to extend the sampling during and eliminate such oscillations. The cycling voltage data is re-

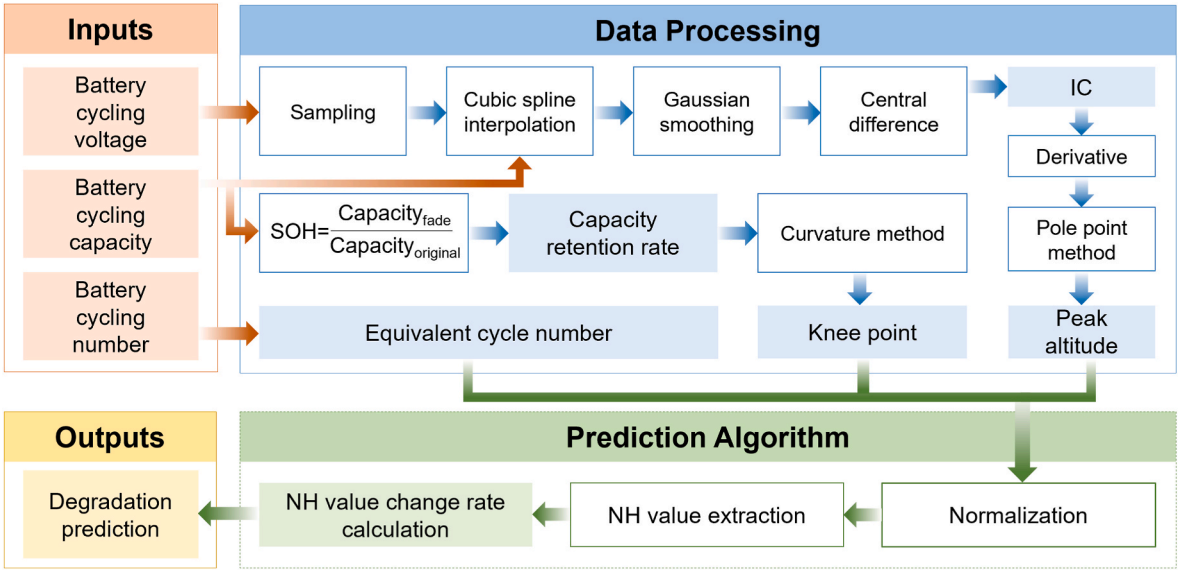

Fig. 1. Flowchart of the MO-DIC analysis method.

sampled first, followed by the sampling capacity data. After resampling, the Gaussian filter method is used to smooth the curve. The Gaussian filter is based on the Gaussian function, defined as followed,

$$G(x) = \frac{1}{\sigma\sqrt{2\pi}} \exp\left(-\frac{(x-\mu)^2}{2\sigma^2}\right) \quad \text{Eq. 4}$$

This function decreases the probability distribution of the function. When used for curve smoothing, the value of each sampled data point is recalculated based on the values of other nearby points. The Gaussian function states that the closer a given point is to the sampling point, the greater its influence on the sampling point value (and vice-versa). Thus, the value for each sampled point can be found by:

$$y_{sampling\ point} = \sum_{i=n-r}^{n+r} y_i * G(x) \quad \text{Eq. 5}$$

where n is the location of the sampling point, and r is the number of nearby points within half of the target length. The recalculated value for each sampling point can then be obtained by conducting convolution. Following this, the IC value can be calculated using the central difference method. The IC curve can then be used to analyze or highlight key features. To numerically analyze these features, such as the change of the curve's peak, for example, for the derivative of the IC can be calculated, using:

$$\frac{d}{dV}\left(\frac{dQ}{dV}\right) = \frac{d^2Q}{dV^2} \quad \text{Eq. 6}$$

3. Experimental

3.1. Battery Assembling

To investigate the nonlinear decay issues of the NCM622/graphite system battery, the pouch batteries (nominal capacity of 25 Ah@1 C) were examined. They contained a NCM622 cathode material (Ningbo Ronbay Lithium Battery Material Co., Ltd., China) and a graphite anode material (Shenzhen BTR New Energy Materials Co., Ltd., China). The cathode electrodes were made from NCM, and had compositions of 97.5 wt% active material, and 2.5 wt% carbon black and carbon nanotubes, with the remainder comprising a polyvinylidene fluoride (PVDF) binder. The anode electrodes were 95.7 wt% graphite and 1.6 wt% carbon black, as well as 2.7 wt% styrene-butadiene rubber and a carboxymethyl batteryulose binder. The ratio of the active material's capacity in the anode electrode to that in the cathode was 1.1:1. A polypropylene-coated ceramics separator (16 μm thickness; Shenzhen Star Source Material Polytron Technologies Co., Ltd., China) was used in between the two electrodes. The batteries were sealed in an all aminated polymer film box. After being vacuum dried at 110 °C for 12 h, they were directly transferred to a dry room (dew-point temperature: ≤ −40 °C), where they were filled with 142 g of electrolyte (LBC435B10; Shenzhen Capchem Technology Co., Ltd., China).

To validate our approach, we concurrently fabricated lithium-ion batteries with an N/P ratio of 0.9, which are highly prone to lithium plating. These batteries exhibit a more pronounced non-linear capacity degradation knee point at the end of their cycling life. By adjusting the anode areal density during electrode sheet coating, we created batteries with varying tendencies for lithium plating. Specifically, we compared batteries with an N/P ratio of 1.1, referred to as Battery Test (BT), which were used for aging degradation detection in our initial method, to those with an N/P ratio of 0.9, referred to as Battery Validation (BV), which served as a control group to study the non-linear capacity degradation characteristics under micro-overcharging conditions.

3.2. Electrochemical testing

The BT batteries, subjected to the testing method, were designated as BT-4.3V and BT-4.4V based on their respective maximum charging voltages. Capacity testing of the BT batteries included constant current-constant voltage (CC-CV) charging and CC discharging. During CC-CV charging, the batteries were charged at a CC rate of 1C until they reached 4.3 V or 4.4 V. Subsequently, CV charging was employed until the battery current decayed to 0.05C. For the CC discharging process, a constant current rate of 1C (equivalent to 25 A) was used to discharge the batteries down to 2.8 V. The BV-4.4V battery was subjected to a specific testing protocol. Initially, the battery underwent 48 cycles of normal cycling tests, which included CC-CV charging at a 1C rate to a charge cutoff voltage of 4.2 V, and then holding at 4.2 V until the current decayed to 0.05C. This was followed by a 0.5-h rest and discharging at 1C to 2.8 V. Subsequently, the charge cutoff voltage was adjusted to 4.4 V, and the battery underwent 2 cycles of micro-overcharge cycling. After completing these 2 micro-overcharge cycles, the battery resumed normal cycling tests. This alternating pattern between high-rate and micro-overcharge cycling tests was maintained until the battery reached its end-of-life. The Open-Circuit Voltage (OCV) tests for the BT-4.2V, BT-

4.3V, and BT-4.4V batteries are conducted as follows: The batteries are charged or discharged at a 1C current rate. After each adjustment of 10 % SOC, the batteries are allowed to rest for 3 h. The voltage value recorded after this rest period is taken as the OCV value for the corresponding SOC state. All electrochemical tests of the batteries were conducted at a temperature of 25 °C ± 2 °C and a relative humidity of 10 %–90 % until a rapid capacity fade was observed, unless otherwise specified.

3.3. Post-mortem analysis

The discharged failed batteries were subsequently introduced into a glove box purged with nitrogen, a measure taken to shield the batteries from the deleterious effects of humidity. Within this controlled environment, the outer aluminum-plastic film was carefully excised using non-reactive ceramic scissors, in order to prevent any unwanted interactions with moisture or atmospheric oxygen. The cathode and anode electrode were then extracted and placed into a glass container containing dimethyl carbonate (DMC), where they were allowed to soak for 30 min. A syringe filled with DMC was then used to perform secondary cleanings of both of the electrodes' surfaces. After these were allowed to dry in the glove box for 1 h, a non-woven cloth moistened with N-methyl-2-pyrrolidone (NMP)was used to gently wipe one side of each electrode until the active material was completely removed on that side. The electrodes were punched into small round discs using a die-punch machine with a 14 mm hole diameter. The cathode discs were placed into a vacuum glove box at 80 °C for 6 h to bake, while the anode discs were baked in a vacuum glove box at 65 °C for 6 h. The anodes and cathodes were then reassembled into button batteries. The resultant NCM/Li half-batteries were tested using CC-CV charging up to 4.4 V, and CC discharging down to 2.8 V, both at 0.05 C. The same process was used for the graphite/Li half-batteries, with charging cut-off at 2.0V and discharging to 0.05 V, also at 0.05 C.

Inductively-Coupled Plasma (ICP) spectroscopy was used to quantify the surface concentrations of Ni, Co, and Mn. This technique was selected to detect potential dissolution of cathode materials and their subsequent deposition on the anode, which could indicate material degradation. Additionally, Gas chromatography-mass spectrometry (GC-MS) was used to analyze the internal gases extracted from the failed batteries. The aim was to identify and quantify the gases produced within the battery, which could be indicative of certain chemical reactions or degradation processes.

4. Results and discussion

4.1. Cycling performance of the test batteries

The comparative analysis of lithium-ion batteries with N/P ratios of 1.1 and 0.9 within this study was conducted to discern the impact of these ratios on battery performance, particularly focusing on the degradation characteristics. The voltage-capacity profiles illustrated in Fig. 2(a) highlight that the battery with an N/P ratio of 1.1 (black curve) maintains a more stable voltage platform and higher discharge capacity throughout its cycling life. This stability is indicative of a balanced lithium-ion intercalation and deintercalation process, which is essential for sustained battery performance. Conversely, the battery with an N/P ratio of 0.9 (red curve) displays a more rapid voltage decline during discharge, resulting in a lower discharge capacity. This observation suggests that a lower N/P ratio may lead to a quicker attainment of the cutoff voltage during discharge, thereby diminishing the battery's energy output. Fig. 2(b) provides a comparative view of the capacity retention and cycling efficiency for both battery types over their entire lifecycle. Notably, the battery with an N/P ratio of 0.9 exhibits more frequent fluctuations in discharge efficiency. These fluctuations are

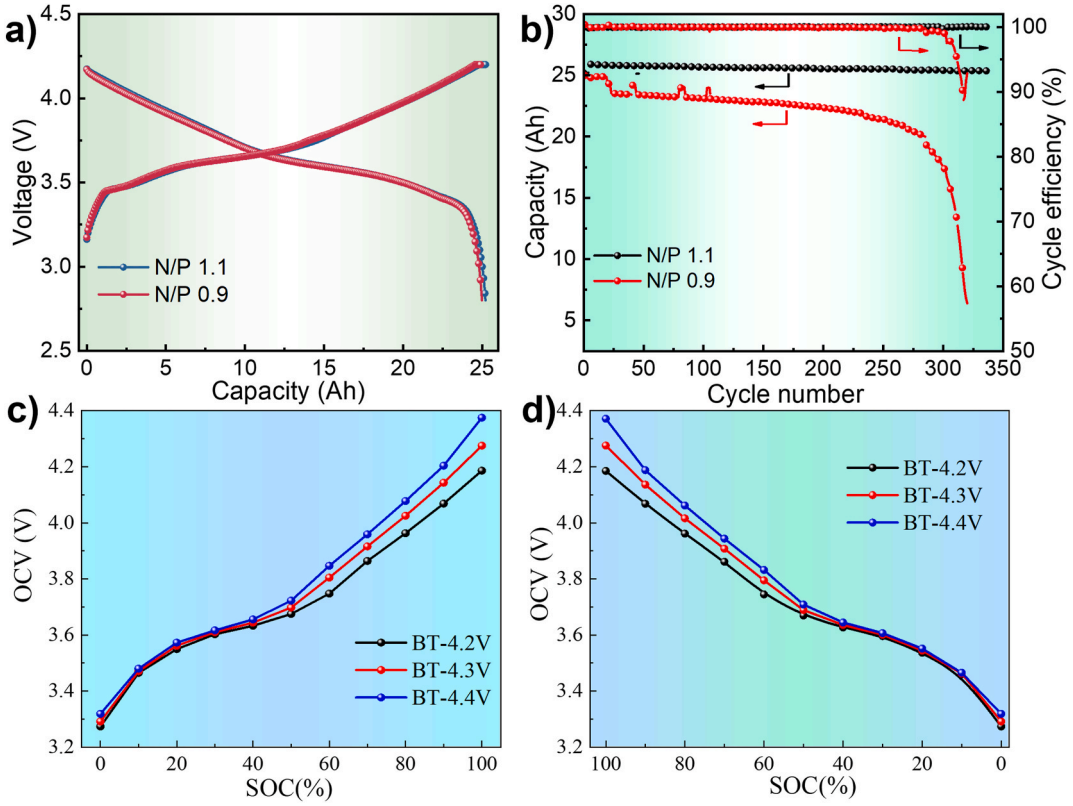

Fig. 2. Charge/discharge profiles of the tested pouch battery: (a) voltage-capacity curve (b) cyclic capacity and efficiency; (c) OCV curves of BT-4.2V, BT-4.3V, and BT-4.4V batteries at different SOC levels during the charging process; (d) OCV curves of BT-4.2V, BT-4.3V, and BT-4.4V batteries at different SOC levels during the discharging process.

likely attributable to an increased propensity for lithium plating, which is particularly pronounced in batteries with lower N/P ratios. The significant nonlinear capacity degradation observed in these batteries is associated with insufficient active anode material, leading to localized lithium deposition during cycling. This localized lithium deposition not only elevates the internal resistance of the battery but also contributes to the gradual structural disintegration within the battery. As the cycle count increases, this structural breakdown results in a rapid capacity decline, signaling the battery's transition into its end-of-life phase.

To compare the charging characteristics of BT-4.2V, BT-4.3V, and BT-4.4V batteries, we determined their 1C discharge capacities to be 24.6 Ah, 25.5 Ah, and 26.7 Ah, respectively. Additionally, we measured the OCV variation patterns during both charging and discharging processes at various SOC levels, which allowed us to discern the distinct electrochemical behaviors associated with each battery type under different charging conditions. Fig. 2(c) and (d) illustrate OCV curves for BT-4.2V, BT-4.3V, and BT-4.4 V batteries, during the charging and discharging processes, respectively. Notably, the OCV curves converge when the SOC is below 50 %, suggesting similar electrochemical responses in this range. In contrast, above 50 % SOC, the curves diverge markedly, indicating varying electrochemical processes and degradation mechanisms at higher SOC levels. At SOC levels above 50 %, the increased voltage can lead to several detrimental effects. These higher voltages can cause excessive side reactions, such as the oxidation of electrolytes and the subsequent thickening of the solid electrolyte interphase (SEI) layer. This thickening can trap more lithium ions, leading to a loss of active lithium inventory and a decrease in the battery's overall capacity. Additionally, the higher voltage can accelerate the dissolution of transition metals from the cathode, which can then deposit on the anode, further contributing to capacity loss and potential short-circuiting. Therefore, it is evident that the micro-overcharging of 4.3V and 4.4V batteries significantly amplifies the characteristics of battery capacity change, offering a clearer perspective on the nonlinear degradation process. This amplification is pivotal for investigating and anticipating capacity fade, as it brings to light a more distinct indication of the degradation mechanisms, especially in the context of nonlinear capacity degradation in batteries.

4.2. *Non-linear degradation characteristics analysis of micro-overcharged batteries*

Based on previous research, the capacity loss of the cathode is primarily attributed to structural degradation, as evidenced by the deterioration of the crystal structure over cycles, which leads to a decrease in specific capacity [29]. The formation of secondary phases and the dissolution of active material also contribute to this loss. For the anode, capacity loss is mainly due to the formation and growth of the solid electrolyte interphase layer [30]. The loss of active lithium, observed throughout the battery's life, is primarily caused by irreversible reactions between lithium ions and the electrolyte, resulting in the formation of SEI and other by-products [31]. Fig. 3(a) shows the IC curves of the battery after varying cycle numbers, each refer to cycles at 1 C. Between cycles 20–140, the battery IC curve had three distinct peaks, labeled1*, 2*, and 3* (Fig. 3(a)). According to the results of previous relevant studies [32], peak 1*is related to the anode, while peaks 2* and 3* are associated with the cathode NCM. The curve indicates that, prior to 160 cycles, peak 1* remained unchanged, the height of peak 2* decreased, and the position of peak 3 moved towards a higher potential-suggesting that the degradation of the battery during this stage was mainly related to the loss of the cathode. However, after 160 cycles, both the positions of peaks 1* and 2* shifted toward higher potentials, and the intensities of both peaks decreased, with peak 3* disappearing. This indicated that, at this point, loss of both the anode and cathode materials, as well as the lithium inventory, had occurred, By the time the battery reached 180 cycles, it had failed completely, with no peaks present in its IC curve. Fig. 3(b) shows its DV curves where, after 160 cycles, the positions of peaks l# and 2# had moved toward lower capacity values. Fig. 3(b) presents the DV curves, where Ql, Q2, and Q3 correspond to the capacity values associated with anode material capacity loss, active lithium capacity loss, and cathode material capacity loss, respectively. After 160 cycles, both the anode and cathode materials suffered significant losses, and the amount of lost active lithium had exceeded the loss of both the anode and cathode materials (Fig. 3(c)). This discrepancy is primarily due to the fact that the layered NCM cathode undergoes accelerated transition-metal dissolution during the initial 140 cycles under high-voltage cycling. The dissolved $Ni^{2+}/Co^{2+}/Mn^{2+}$ ions migrate to the anode and plate on the graphite surface, which initially dominates the capacity fade due to cathode mass loss. In the early cycles, the contributions of anode and lithium loss are below the resolution of the test equipment and are statistically set to zero. In later cycles, the situation changes. The plated metals catalyze continuous electrolyte reduction, which thickens the SEI layer and traps additional Li^{+}. Concurrently, the intercalation of metals into the graphite lattice distorts its structure, increasing impedance and accelerating graphite pulverization. Thus, while the dissolution of the cathode is the primary trigger for degradation, the metals released subsequently drive both the depletion of lithium inventory and the structural failure of the anode. As a result, all three loss mechanisms become operative in the later cycles.

Post-failure testing of the battery revealed the specific capacities of the cathode and anode materials, with results shown in Table 1. The specific capacity values for both the electrode materials stabilized after cycle 6. Analysis of the data indicates that at a cut-off voltage of 4.4 V, the specific capacity of the cathode material decreased by 18.20 mAh/g ±3 mAh/g, while that of the anode material decreased by 50.59 mAh/g ± 2 mAh/g. Consequently, the specific capacity loss rates for the cathode and anode materials were 9.45 % ± 1.55 % and 15.3 % ± 0.6 %, respectively.

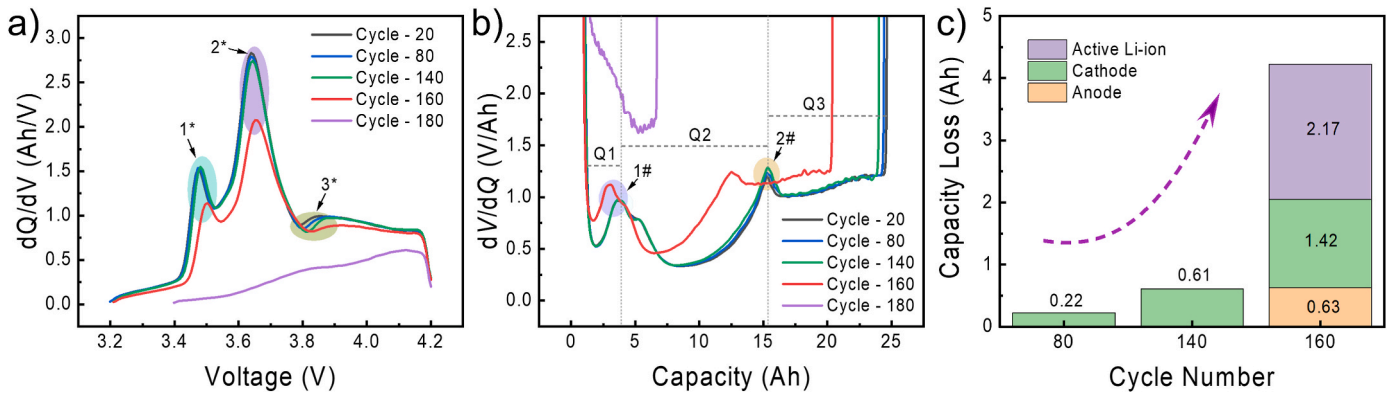

Fig. 3. Incremental capacity curve analysis of battery capacity fade sources: (a) IC curves, (b) DV curves, and (c) sources of capacity loss at different cycles.

Table 1
Capacity loss test results of cathode and anode materials in the failed batteries.

Electrode	Discharge capacity [mAh/g]		Total capacity loss [mAh/g]	Specific capacity loss ratio [%]
	Initial	Failed		
Cathode	192.58	175.63	18.20 ± 3	9.45 ± 1.55
	192.56	171.44		
	192.78	176.24		
Anode	330.35	280.17	50.59 ± 2	15.3 ± 0.6
	330.52	281.48		
	330.24	277.7		

After failure, a significant quantity of gas was produced, causing the battery to bulge, as shown in Fig. 4(a). Following failure, the anode electrode sheet displayed both yellow and black areas. The yellow regions were likely associated with lithium salts or lithium-carbon compounds, as shown in Fig. 4(b). By contrast, the cathode surface appeared more uniformly colored, as shown in Fig. 4(c). GC-MS analysis of the gas produced in the battery indicated a composition of hydrogen, oxygen, nitrogen, and hydrocarbon gases, with percentages of 78 %, 2 %, and 6 %, respectively (Fig. 4(d)). The presence of oxygen and nitrogen was possibly due to air infiltration into the gas collector. Because hydrogen was the primary gas produced by reactions in the lithium-ion batteries, this failure mechanism was possibly related to hydrogen generation.

Analysis of the anode material from the failed battery revealed the significant presence of Ni, Co, and Mn, as shown in Fig. 4(e). By contrast, these elements were not detected in the anode material of the normal operating battery. Throughout the cycling process with mild overcharge, the battery's cathode material experienced excessive metal dissolution, leading to deposition on the anode. Previous research found that Ni ions from this dissolution deposited on the negative electrode, forming metallic nickel, which contributed to the catalytic production of hydrogen gas [33]. Concurrently, metal dissolution at the cathode could also result in degradation of the solid electrolyte interphase film on the anode's surface, accelerating active lithium loss. This degradation ultimately resulted in the complete loss of active lithium, as well as the active materials of the anode and cathode. Consequently, we inferred that the battery's failure process commenced with high voltage conditions that induced excessive metal dissolution in its cathode material. The dissolved metal ions likely migrated to the anode, where they deposited and subsequently destabilized the SEI on the anode's surface. The ongoing formation and degradation of the SEI membrane then contributed to the depletion of active lithium. Deposited nickel also likely facilitated hydrogen gas generation through the catalysis of protonated byproducts. These factors were likely responsible for the capacity changes during the cycling process, which exhibited nonlinear degradation characteristics.

4.3. MO-DIC curve analysis of the micro-overcharged batteries

The identification of knee points in the capacity fade curve is considered instrumental in analyzing the onset of rapid capacity decline in batteries. However, discerning other indicative features before this juncture can be challenging. Prior to the knee point, health life value experiences a gradual decline, which may be difficult to identify. Therefore, non-destructive prediction of the knee point relies on identifying these subtle capacity fade characteristics.

To determine the anticipatory benefits of MO-DIC values in forecasting battery capacity knee point, a comparative analysis was performed on the MO-IC and MO-DIC curves as a function of voltage across diverse cycles for the BT-4.4 V and BT-4.3 V batteries. As shown in Fig. 5 (a), prior to the knee point (cycle 161), the initial peak in the IC diagram of the BT-4.4 V battery on the left demonstrated a decrease in peak value and a right shift in position. This suggested that the aging characteristics evolved in tandem with the cycle count, mirroring the trends observed in the capacity fade curve. Based on this peak's value and position, it was possible to extract an MO-IC feature before the knee point, which could be used to predict the knee point using a measurement-based approach rather than the model-based approach. This measurement-based approach would be much easier to deploy in an EV, for example, because it does not rely on the complex computations needed in a battery aging model. However, a single MO-IC curve is not suitable for making accurate predictions, because the shapes of the peaks (i.e., first peak in Fig. 5(a)) will change as a battery ages, resulting in decreases in their maximum values. Therefore, it was beneficial to continue processing this curve to better highlight this signal. Fig. 5(b) presents the MO-DIC curve of the BT-4.4 V battery, showing 2 peaks and 2 valleys, with peak and valley intensities about 10 times higher than those in the MO-IC curve of Fig. 5(a). In Fig. 5(b), the intensity of peaks and valleys declines with battery aging, while the corresponding voltage increases. This indicates that the MO-DIC curve is more sensitive to the aging process and is better suited for calculating battery life cycle knee point.

Fig. 5(c) and (d) presents the MO-IC and MO-DIC curves for the BT-4.3 V battery, providing an in-depth analysis of the battery's electrochemical behavior throughout the cycling process. The MO-IC curve for the BT-4.3 V battery, as shown in Fig. 5(c), exhibited a less pronounced initial peak and more significant rightward shift compared to the BT-4.4 V battery shown in Fig. 5(a). Similarly, the MO-DIC curve for the BT-4.3 V battery in Fig. 5(d) demonstrated peak heights that were consistent with those of the BT-4 V battery, though with a more pronounced

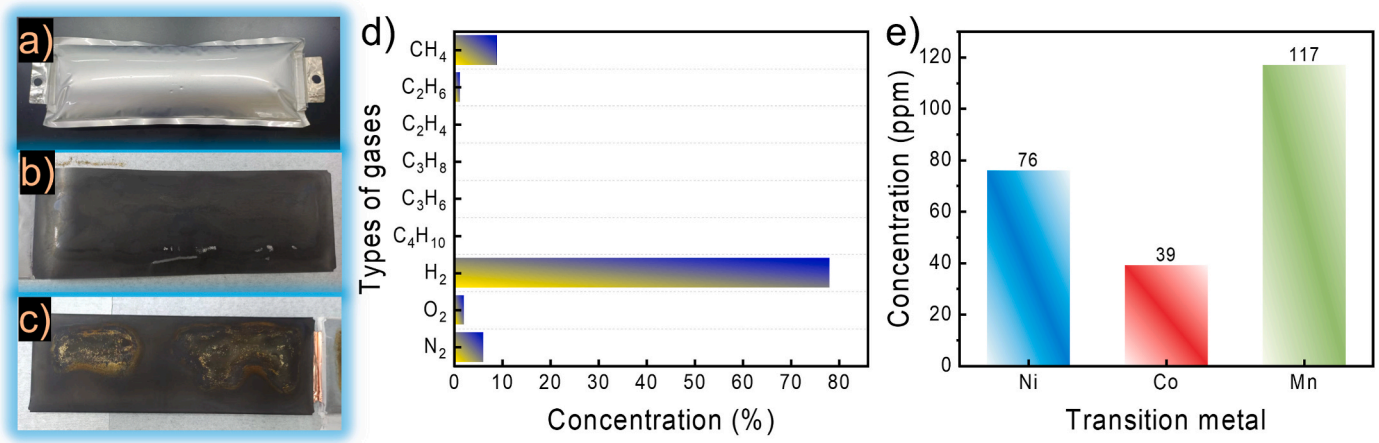

Fig. 4. Post-mortem analysis of the failed battery: (a) bulging battery after failure, (b) and (c) the positive and negative electrodes, respectively, d) gas composition, and (e) transition metal content in the anode post-failure.

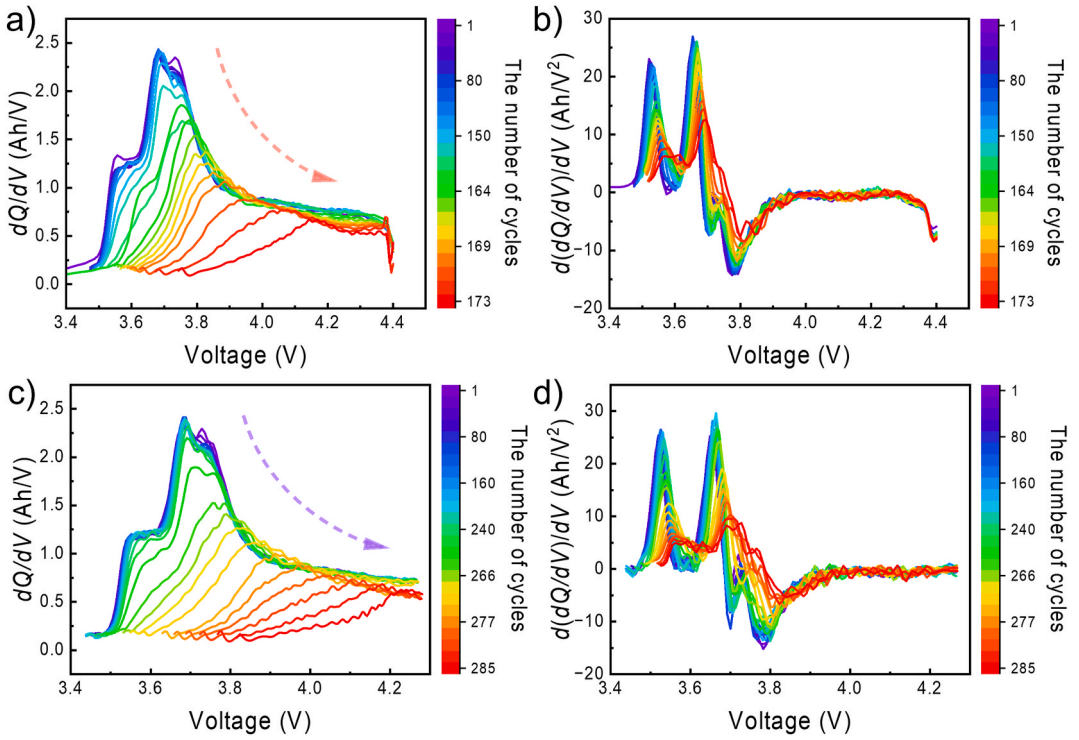

Fig. 5. MO-IC and MO-DIC curves of the BT-4.4 V and BT-4.3 V batteries: (a) BT-4.4 V IC curve, (b) BT-4.4 V DIC curve, (c) BT-4.3 V IC curve, and (d) BT-4.3 V DIC curve.

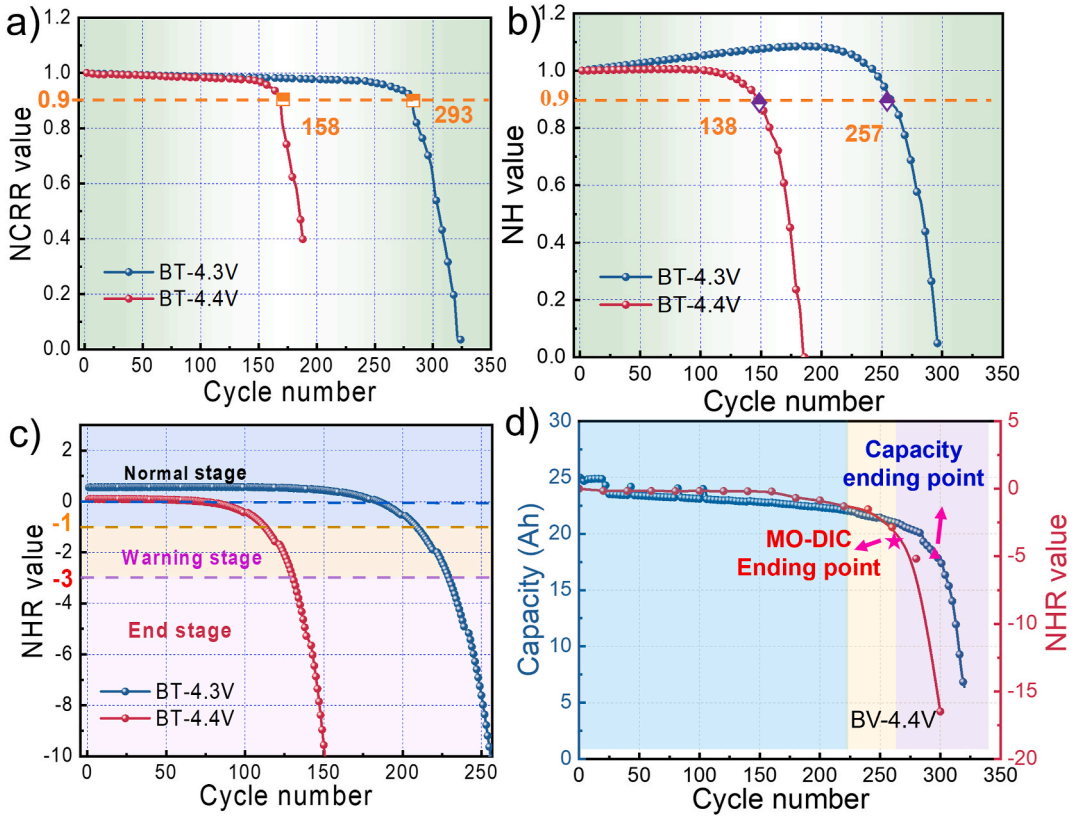

Fig. 6. MO-DIC analysis of the BT-4.3 V and BT-4.4 V batteries: (a) variation in the normalized capacity retention rate (NCRR) with number of cycles, (b) variation in the normalized peak height (NH) value of the MO-DIC method with number of cycles, (c) variation in the normalized peak height change rate (NHR) with number of cycles. (d) Comparative analysis of capacity fade and NHR value variations throughout cycling. Validation of the MO-DIC variation of BV-4.4V

rightward shift. The distinct peaks in the MO-DIC curve, especially for the BT-4.4 V battery, offered more reliable features for detailed analysis and predictive modeling of battery health and longevity.

To determine the utility of the peak height in the DIC curve for predicting the battery's knee point, a correlation was established between the peak height of the MO-DIC curve and cycle count. To ensure the strategy's repeatability and applicability to other batteries, the second peak height of the MO-DIC curve was selected and normalized using Equation (1), denoted the normalized peak height (NH value):

$$NH_i = \frac{H_i}{H_1}, \quad \text{Eq. 7}$$

where NH_i represents the normalized peak height of the MO-DIC curve at the ith cycle, and H_i and H_1 denote the peak heights at the ith and 1st cycles, respectively. To compare the capacity retention rate with the MO-DIC peak heights, the capacity retention rate was also normalized, as follows, and denoted the normalized capacity retention rate (NCRR):

$$NCRR_i = \frac{CRR_i}{CRR_1}, \quad \text{Eq. 8}$$

where $NCRR_i$ is the normalized value for the capacity retention rate at the ith cycle, and CRR_i and CRR_1 represent the capacity retention rates at the ith and 1st cycles, respectively.

Post normalization, the MO-DIC peak heights for both the BT-4.3 V and BT-4.4 V batteries exhibited similar trends, as shown in Fig. 6(b), and a clear pattern of advanced decrease compared to the capacity retention rate curves, as shown in Fig. 6(a). This characteristic could be employed to predict the knee point, identified at cycle 158 for the BT-4.4 V battery and cycle 293 for the BT-4.3 V battery. To demonstrate the predictive capability of this strategy, a threshold of 0.9 was selected as a feature value for the peak height. The cycle number at this value was recorded, which was cycle 275 for the BT-4.3 V battery and 138 for the BT-4.4 V battery. This indicated that the DIC peak height feature value appeared after 36 cycles for the BT-4.3 V battery and 20 cycles for the BT-4.4 V battery before their knee points, as shown in Table 2. Manifestation of the MO-DIC peak height feature occurred 20–36 cycles prior to the battery's capacity knee point, indicating that the MO-DIC method could predict the lifespan with an advance of approximately 13 % of the cycle life. This early detection of the MO-DIC knee point suggested that MO-DIC was more sensitive to the initial stages of degradation due to aging processes such as LAM depletion, which was accentuated by the micro-overcharging strategy. To achieve real-time lifespan prediction for batteries, especially those exhibiting nonlinear capacity changes, we extracted and analyzed the peak height change rate (NHR value) in the MO-DIC method on a cycle basis, and found that the NHR value not only mirrored the trend of the NH value but also exhibited a more monotonically smooth variation with increasing cycle numbers, making it a suitable characteristic parameter for assessing the changes in battery life cycle, as shown in Fig. 6(c). The calculation formula is given by Equation (9).

$$NHR_i = \frac{NH_i}{NH_{i+1}} \times 1000. \quad \text{Eq. 9}$$

Consequently, we established a benchmark NHR value as an indicator of the battery's non-linear decay inflection point. By conducting a comprehensive analysis of Fig. 6(a)–6(c), we could define the lifecycle states of the batteries experiencing nonlinear capacity degradation based on the NHR value across different ranges. When the NHR value exceeded −1, the battery was considered to be in a normal operational state. However, when the NHR value fell between −1 and −3, the battery approached its end of life. When the NHR value was less than −3, the battery capacity diminished rapidly, indicating that it had reached its end of life.

Table 2
Knee points of the battery, in terms of the capacity and derivative of incremental capacity.

battery number	Cut-off voltage	Capacity knee point	MO-DIC knee point	Cycle difference
BT-4.3 V	4.3 V	293	257	36
BT-4.4 V	4.4 V	158	138	20
BV-4.4 V	4.4 V	439	389	50

To thoroughly validate the applicability of our method and to confirm its accuracy in predicting battery life, we subjected BV-4.4V batteries to routine cycling until failure. During this process, MO-DIC tests were conducted twice following every 48 regular cycles to calculate the NHR value. Fig. 6(d) presents the curves of capacity degradation and NHR value changes observed in this test. It is evident that the battery maintained a relatively stable operational status for the first 330 cycles. Subsequently, the NHR value began to decline significantly, indicating that the battery had entered the designated warning zone. This zone lasted for approximately 50 cycles before the battery rapidly transitioned into its end-of-life stage. Continuing to use the battery at this point could result in a sudden and drastic drop in capacity, potentially leading to battery failure. These observations suggest that the predictive cycles can be advanced by approximately 50 cycles compared to the capacity degradation trend, with the end-of-life of the batteries determined by the NHR value falling below −3 and the capacity fade reaching 80 %, respectively.

The MO-DIC method could be easily applied and integrated into the BMS of electric vehicles. As outlined in the flowchart of Fig. 7, initiating with standard operational procedures, the vehicle's battery experienced normal discharge and charge cycles, and then two MO-DIC cycles could be designed to obtain critical data for subsequent analysis. After MO-DIC cycles, the calculation of the incremental capacity (IC) curve's derivative should be executed, and the NH value could be extracted from the MO-DIC peak height to evaluate the battery's health and forecast its end-of-life trajectory. Additionally, the NHR value was calculated to quantitatively measure the battery's degradation status. This analysis concluded with a result signal that fed into the BMS, allowing the system to make proactive decisions regarding battery usage, maintenance, or replacement. This methodological approach, as delineated in the flowchart, not only refined the BMS's predictive acumen, but also underscored the promising prospects of the MO-DIC method in enhancing the longevity and reliability of EV batteries. By providing early detection indicators of degradation, the MO-DIC method could become a cornerstone for the advancement of battery health management, ensuring sustained performance, and the overall efficiency of battery systems in EVs. Despite the fact that multi-stage charging protocols are commonly used in the practical application of batteries or battery packs, MO-DIC method can be employed at specific time points to accurately assess battery life degradation. For instance, during the regular maintenance of EVs, a single test using the MO-DIC method can provide predictive data on the current battery life degradation. Combined with historical data from the database, this enables us to precisely calculate the current health status of the battery. In future research, we will accumulate more data to further optimize and enhance the accurate prediction capability of the MO-DIC method.

In summary, the MO-DIC method enhanced the predictive sensitivity and accuracy of the BMS, thus, advancing the safe and reliable operation of EVs. This approach could become a cornerstone in the evolution of battery health management, ensuring the sustained performance and overall efficiency of EV systems.

5. Conclusions

This study has successfully demonstrated the critical influence of micro-overcharging on the nonlinear capacity degradation of lithium-ion batteries, particularly when the N/P ratio is suboptimal. By conducting a thorough analysis of batteries with N/P ratios of 1.1 and 0.9, we have identified distinct degradation patterns that significantly

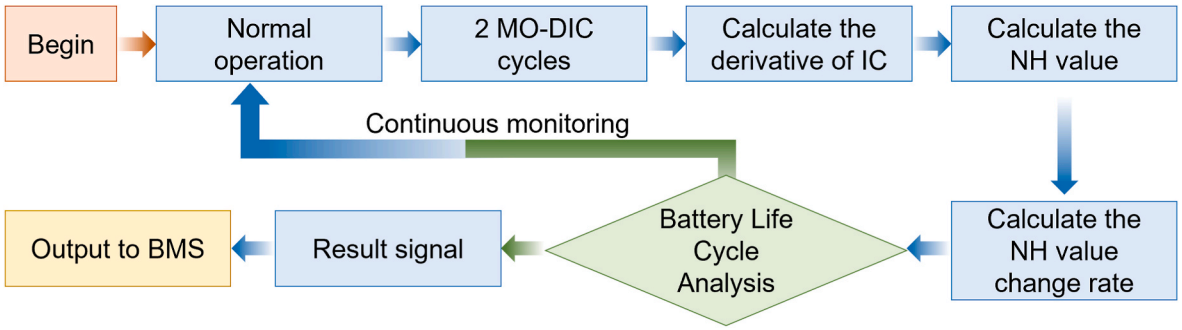

Fig. 7. Schematic diagram of BMS in electric vehicles using the MO-DIC method for battery prediction.

impact battery performance and longevity. The results indicate that prolonged micro-overcharging, often associated with lower N/P ratios, accelerates cathode material degradation, leading to a pronounced nonlinear decay in battery capacity. This degradation is characterized by distinct peaks in the incremental capacity (IC) curve, which serve as critical indicators of the battery's health status. The capacity loss, primarily driven by cathode material degradation, underscores the importance of managing charging conditions to mitigate performance decline.

Based on these observations, we introduced the micro-overcharging differential incremental capacity (MO-DIC) method, a novel approach to predict the capacity decay knee point. This method leverages the rate of change of the normalized peak height in the differential overcharging IC curve to provide early warnings of imminent capacity degradation. The validation of MO-DIC using low N/P ratio batteries revealed its ability to detect the degradation knee point several cycles ahead of traditional indicators, enhancing proactive battery health management and potentially extending battery life. Routine cycling tests on BV-4.4V batteries, conducted until failure with MO-DIC tests performed every 48 cycles, confirmed the method's efficacy. MO-DIC demonstrated its capability to forecast the battery's life inflection point 25 to 36 cycles ahead of capacity fade indicators and approximately 50 cycles before reaching end-of-life. This advanced prediction capability is a significant advancement in battery health status prediction, offering substantial benefits for battery life cycle analysis and the formulation of proactive maintenance strategies.

In conclusion, the MO-DIC method presents a robust tool for predicting nonlinear capacity degradation in lithium-ion batteries, particularly under conditions of micro-overcharging. Its ability to provide early warnings of battery degradation can significantly enhance battery management practices and extend operational lifespans. Future research will continue to refine the MO-DIC method and assess its applicability across various battery types and operating conditions, aiming to further improve its predictive accuracy and practical utility. This study's findings contribute to the broader understanding of battery degradation mechanisms and pave the way for more effective battery management strategies in the electric vehicle and energy storage sectors.

CRediT authorship contribution statement

Xiaoli Ma: Writing – original draft, Investigation, Data curation. **Sheng Fang:** Writing – original draft, Methodology, Data curation. **Xueling Shen:** Supervision, Resources, Methodology. **Hang Zhang:** Visualization, Validation. **Fengling Yun:** Methodology, Formal analysis. **Min Gao:** Validation, Software. **Zhanglong Yu:** Writing – review & editing, Formal analysis, Data curation. **Yanyan Fang:** Writing – review & editing, Funding acquisition, Conceptualization. **Fang Lian:** Writing – review & editing, Supervision, Conceptualization.

Declaration of generative AI and AI-assisted technologies in the writing process

The authors declare that they did not take advantage of Generative AI and AI-assisted technologies in the writing process.

Declaration of competing interest

The authors declare that they have no known competing financial interests or personal relationships that could have appeared to influence the work reported in this paper.

Acknowledgments

This work was supported by Beijing Natural Science Foundation [grant number L243020].

Data availability

Data will be made available on request.

References

[1] Viswanathan V, Epstein AH, Chiang YM, Takeuchi E, Bradley M, Langford J, Winter M. The challenges and opportunities of battery-powered flight. Nature 2022;601:519–25. https://doi.org/10.1038/s41586-021-04139-1.
[2] Han S, Han Y, Liu S, Liu Y, Yang X, Feng K. VBO_3/V_2O_3@C heterogeneous anode material with high-specific-capacity and high-stability for lithium-ion batteries. J Energy Storage 2024;101:113990. https://doi.org/10.1016/j.est.2024.113990.
[3] Wang Y, Du G, Han D, Shi W, Deng J, Li H, Zhao W, Ding S, Su Q, Xu B. Mg/Fe site-specific dual-doping to boost the performance of cobalt-free nickle-rich layered oxide cathode for high-energy lithium-ion batteries. J Energy Chem 2024;91:670–9. https://doi.org/10.1016/j.jechem.2024.01.031.
[4] Yang M, Sun X, Liu R, Wang L, Zhao F, Mei X. Predict the lifetime of lithium-ion batteries using early cycles: a review. Appl Energy 2024;376:124171. https://doi.org/10.1016/j.apenergy.2024.124171.
[5] Atalay S, Sheikh M, Mariani A, Merla Y, Bower E, Widanage WD. Theory of battery ageing in a lithium-ion battery: capacity fade, nonlinear ageing and lifetime prediction. J Power Sources 2020;478:229026. https://doi.org/10.1016/j.jpowsour.2020.229026.
[6] Lee H, Seok J, Chung C, Park S, Kim J, Yoon W-S. Impact of high-temperature storage on capacity fading of Ni-rich cathodes in sulfide-based all-solid-state batteries. Chem Eng J 2024;498:154903. https://doi.org/10.1016/j.cej.2024.154903.
[7] Wang Y, Zhu J, Cao L, Gopaluni B, Cao Y. Long short-term memory network with transfer learning for lithium-ion battery capacity fade and cycle life prediction. Appl Energy 2023;350:121660. https://doi.org/10.1016/j.apenergy.2023.121660.
[8] Attia PM, Bills A, Planella FB, Dechent P, dos Reis G, Dubarry M, Gasper P, Gilchrist R, Greenbank S, Howey D, Liu O, Khoo E, Preger Y, Soni A, Sripad S, Stefanopoulou AG, Sulzer V. Review-"Knees" in lithium-ion battery aging trajectories. J Electrochem Soc 2022;169:060517. https://doi.org/10.1149/1945-7111/ac6d13.
[9] Dubarry M, Baure G, Anseán D. Perspective on state-of-health determination in lithium-ion batteries. J Electrochem Energy Convers Storage 2020;17:044701. https://doi.org/10.1115/1.4045008.
[10] Wang M, Wu S, Chen Y, Luan W. The snowball effect in electrochemical degradation and safety evolution of lithium-ion batteries during long-term cycling. Appl Energy 2025;378:124909. https://doi.org/10.1016/j.apenergy.2024.124909.
[11] Hu XS, Xu L, Lin XK, Pecht M. Battery lifetime prognostics. Joule 2020;4:310–46. https://doi.org/10.1016/j.joule.2019.11.018.

[12] Yifan Z, Sida Z, Zhengjie Z, Xinan Z, Rui C, Qiangwei L, Zichao G, Chengcheng F, Shichun Y. A capacity fade reliability model for lithium-ion battery packs based on real-vehicle data. Energy 2024;307:132782. https://doi.org/10.1016/j.energy.2024.132782.
[13] Wang C, Wang R, Liu G, Ji Z, Shen W, Yu Q. Progressive degradation behavior and mechanism of lithium-ion batteries subjected to minor deformation damage. J Energy Storage 2024;101:113992. https://doi.org/10.1016/j.est.2024.113992.
[14] Li X, Fan D, Liu X, Xu S, Huang B. State of health estimation for lithium-ion batteries based on improved bat algorithm optimization kernel extreme learning machine. J Energy Storage 2024;101:113756. https://doi.org/10.1016/j.est.2024.113756.
[15] Ji S, Zhang Z, Stein HS, Zhu J. Flexible health prognosis of battery nonlinear aging using temporal transfer learning. Appl Energy 2025;377:124766. https://doi.org/10.1016/j.apenergy.2024.124766.
[16] Zhang H, Sun H, Kang L, Zhang Y, Wang L, Wang K. Prediction of health level of multiform Lithium sulfur batteries based on incremental capacity analysis and an improved LSTM. Prot Control Mod Power Syst 2024;9:21–31. https://doi.org/10.23919/pcmp.2023.000280.
[17] Spitthoff L, Vie PJS, Wahl MS, Wind J, Burheim OS. Incremental capacity analysis (dQ/dV) as a tool for analysing the effect of ambient temperature and mechanical clamping on degradation. J Electroanal Chem 2023;944:117627. https://doi.org/10.1016/j.jelechem.2023.117627.
[18] Li Y, Guo W, Stroe D-I, Zhao H, Kjær Kristensen P, Rosgaard Jensen L, Pedersen K, Gurevich L. Evolution of aging mechanisms and performance degradation of lithium-ion battery from moderate to severe capacity loss scenarios. Chem Eng J 2024;498:155588. https://doi.org/10.1016/j.cej.2024.155588.
[19] Meng HX, Geng MY, Han T. Long short-term memory network with Bayesian optimization for health prognostics of lithium-ion batteries based on partial incremental capacity analysis. Reliab Eng Syst Saf 2023;236:109288. https://doi.org/10.1016/j.ress.2023.109288.
[20] Wang G, Cui N, Li C, Cui Z, Yuan H. A state-of-health estimation method based on incremental capacity analysis for Li-ion battery considering charging/discharging rate. J Energy Storage 2023;73:109010. https://doi.org/10.1016/j.est.2023.109010.
[21] Edge JS, O'Kane S, Prosser R, Kirkaldy ND, Patel AN, Hales A, Ghosh A, Ai W, Chen J, Yang J, Li S, Pang M-C, Bravo Diaz L, Tomaszewska A, Marzook MW, Radhakrishnan KN, Wang H, Patel Y, Wu B, Offer GJ. Lithium ion battery degradation: what you need to know. Phys Chem Chem Phys 2021;23:8200–21. https://doi.org/10.1039/D1CP00359C.
[22] Fly A, Chen R. Rate dependency of incremental capacity analysis (dQ/dV) as a diagnostic tool for lithium-ion batteries. J Energy Storage 2020;29:101329. https://doi.org/10.1016/j.est.2020.101329.
[23] Seo G, Ha J, Kim M, Park J, Lee J, Park E, Bong S, Lee K, Kwon SJ, Moon S-p, Choi J, Lee J. Rapid determination of lithium-ion battery degradation: high C-rate LAM and calculated limiting LLI. J Energy Chem 2022;67:663–71. https://doi.org/10.1016/j.jechem.2021.11.009.
[24] Liu J, Peng W, Yang M, Jin K, Liu P, Sun J, Wang Q. Quantitative analysis of aging and detection of commercial 18650 lithium-ion battery under slight overcharging cycling. J Cleaner Prod 2022;340:130756. https://doi.org/10.1016/j.jclepro.2022.130756.
[25] Wei M, Ye M, Zhang C, Wang Q, Lian G, Xia B. Integrating mechanism and machine learning based capacity estimation for $LiFePO_4$ batteries under slight overcharge cycling. Energy 2024;296:131208. https://doi.org/10.1016/j.energy.2024.131208.
[26] Bi S, Yu Z, Fang S, Shen X, Cui Y, Yun F, Shi D, Gao M, Zhang H, Tang L, Zhang X, Fang Y, Zhang X. Understanding the combustion characteristics and establishing a safety evaluation technique based on the overcharged thermal runaway of lithium-ion batteries. J Energy Storage 2023;73:109039. https://doi.org/10.1016/j.est.2023.109039.
[27] Jeon B-J, Lee Y-H, Jeong K-M. Unveiling the impact of electrode curvature on N/P ratio variations in cylindrical lithium-ion batteries. Energy Storage Mater 2025;76:104117. https://doi.org/10.1016/j.ensm.2025.104117.
[28] Ghazali AK, Aziz NAA, Hassan MK. Advanced algorithms in battery management systems for electric vehicles: a comprehensive review. Symmetry 2025;17:321. https://doi.org/10.3390/sym17030321.
[29] Zhang L, Huang L, Zhang Z, Wang Z, Dorrell DD. Degradation characteristics investigation for lithium-ion cells with NCA cathode during overcharging. Appl Energy 2022;327:120026. https://doi.org/10.1016/j.apenergy.2022.120026.
[30] Li G, Xue R, Chen L. The influence of polytetrafluorethylene reduction on the capacity loss of the carbon anode for lithium ion batteries. Solid State Ionics 1996;90:221–5. https://doi.org/10.1016/S0167-2738(96)00367-0.
[31] Holtstiege F, Wilken A, Winter M, Placke T. Running out of lithium? A route to differentiate between capacity losses and active lithium losses in lithium-ion batteries. Phys Chem Chem Phys 2017;19:25905–18. https://doi.org/10.1039/C7CP05405J.
[32] Rong D, Zhang G, Sun Q, Hu X. Experimental study on gas production characteristics of electrolyte of lithium-ion battery under pyrolysis conditions. J Energy Storage 2023;74:109367. https://doi.org/10.1016/j.est.2023.109367.
[33] Liu H, Zhao X, Xie Y, Luo S, Wang Z, Zhang X, Zhu L. Insights into capacity fading mechanism and coating modification of high-nickel cathodes in lithium-ion batteries. ACS Appl Mater Interfaces 2022;14:55491–502. https://doi.org/10.1021/acsami.2c14235.